

# Generation of dispersive shock waves by the flow of a Bose-Einstein condensate past a narrow obstacle

A. M. Kamchatnov<sup>1</sup> and N. Pavloff<sup>2</sup><sup>1</sup>*Institute of Spectroscopy, Russian Academy of Sciences, Troitsk, Moscow Region, 142190, Russia*<sup>2</sup>*Université Paris Sud, CNRS, Laboratoire de Physique Théorique et Modèles Statistiques, UMR8626, F-91405 Orsay, France*

(Received 22 November 2011; published 5 March 2012)

We study the flow of a one-dimensional Bose-Einstein condensate incident onto a narrow obstacle. We consider a configuration in which a dispersive shock is formed and propagates upstream away from the obstacle while the downstream flow reaches a supersonic velocity, generating a sonic horizon. Conditions for obtaining this regime are explicitly derived and the accuracy of our analytical results is confirmed by numerical simulations.

DOI: [10.1103/PhysRevA.85.033603](https://doi.org/10.1103/PhysRevA.85.033603)

PACS number(s): 03.75.Kk, 47.40.-x

## I. INTRODUCTION

The flow of a quantum fluid past an obstacle can generate various excitations. In the classical example of liquid He-II these are phonons and rotons introduced by Landau [1] in his theory of superfluidity. According to Landau, superfluidity is lost when the flow velocity past an obstacle or through a capillary tube exceeds the threshold of creation of Cherenkov-like radiation of linear waves (or, in other words, of quantum quasiparticles). In actual experiments where He-II flows through a narrow channel, superfluidity is lost at velocities much lower than what is predicted by the Landau criterium (see, e.g., [2]). This discrepancy between theory and experiment was explained by Feynman [3] as resulting from the nucleation of *nonlinear* excitations: vortex rings generated by the flow past the obstacle.

The same phenomenology is observed in the flow of Bose-Einstein condensates (BECs), either for trapped ultracold atomic vapors or polaritons in semiconductor microcavities, with special features linked to the specific dispersion relation of elementary excitations in these systems: for instance, the Landau critical velocity is the velocity of sound  $c$ , and in two dimensions (2D) the Cherenkov radiation forms an interference pattern located outside of the Mach cone [4–7]. These specificities being taken into account, one observes phenomena similar to those observed in liquid helium: in 2D or 3D flows past obstacles, superfluidity is broken at velocity lower than  $c$  [8,9] because of the nucleation of vortices [10–14] or generation of effectively stable oblique solitons [15–17] (recently observed in experiments with polariton condensates [18,19]), and more complicated dispersive shock waves (DSW) patterns [20–22].

The situation in quasi-1D flows is similar: although generation of vortices or oblique solitons is impossible in this case, dark solitons are still easily generated stable nonlinear excitations [23,24]. Together with DSW, these nonlinear excitations are, as is already the case in higher dimension, keys ingredients for understanding the time-dependent dynamics of guided BECs in presence of obstacles, as experimentally studied in Refs. [25–27]. Besides their interest for studying nonlinear quantum transport, quasi-1D BEC flows have also been suggested as model systems for creating sonic horizons suitable for the experimental observation of acoustic analogs of Hawking radiation [28–34]. In particular, an interesting type of stationary sonic horizon has been identified in Refs. [34,35]. It

corresponds to the situation where an upstream subsonic region is separated from a downstream supersonic one by an obstacle of the form of a  $\delta$  potential (see Fig. 1 and discussion below). The present work is devoted to the study of the dynamics of the formation of this configuration. We show that it can be obtained by launching a BEC wave packet onto a localized obstacle (not necessarily a  $\delta$  peak [36]). When the wave packet reaches the potential, the density typically piles up in front of the obstacle, forming a plateau accompanied by a DSW which is ejected upstream. We study the characteristic features of this DSW in detail (both analytically and numerically) and determine for which parameters (specific to the flow and to the obstacle) the situation just described can be realized.

Theoretical analysis of 1D flows past an obstacle has already been addressed in a number of papers (see, e.g., [35,37–40]). In these papers it was found that there exist two critical velocities  $u_-$  and  $u_+$  ( $u_- < c < u_+$ ). The subcritical flows whose velocity  $u$  is below  $u_-$  are superfluid and generate no excitations in vicinity of the obstacle; the supercritical ones with velocity above  $u_+$  do not generate nonlinear DSW but the Cherenkov radiation is effective and there is no sonic horizon; finally, in the transcritical region, for flows whose velocity  $u$  lies between the two critical values  $u_- < u < u_+$ , DSW are generated, generally speaking at both sides of the obstacle,

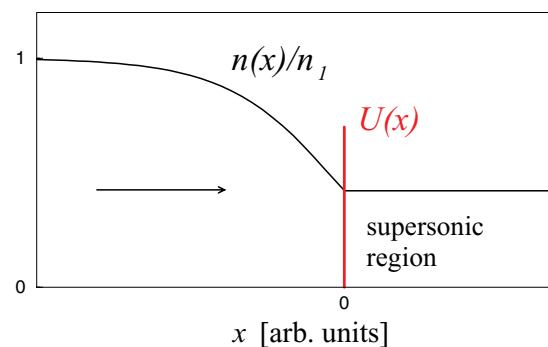


FIG. 1. (Color online) Density profile in vicinity of the  $\delta$  potential represented by a (red) vertical straight line. The flow is stationary, with a velocity directed toward positive  $x$  as indicated by the arrow. The density in the region  $x < 0$  is a portion of a dark soliton (see Sec. III B) with asymptotic upstream density ( $n_1$ ) and subsonic velocity. The flow in the downstream region  $x > 0$  has a constant density and a supersonic velocity.

and only in a very narrow range of velocities both DSW are detached from the obstacle. Hence, it seems difficult to reach a situation such as the one illustrated in Fig. 1.

Note however that the above quoted references [35,37–40] mainly considered flows with identical asymptotic parameters at both sides far enough from the obstacle. This choice of boundary conditions is natural when the obstacle is put into motion starting from a situation where it is immobile in a condensate at rest. However, another setup is possible, which is of considerable practical interest, being similar to the flow of a fluid through a Laval nozzle [41]. In this configuration (already considered in Ref. [42]) the parameters of the flow are kept fixed only on the side of the incoming flow and the downstream flow expands freely into vacuum. In this case a DSW can be created only upstream and the parameters of the shock can be calculated analytically for two typical models of obstacle potential: (i) a smooth potential with typical size greater than the characteristic healing length  $\xi$  and (ii) a short-range potential acting at distances much less than  $\xi$ . In the first case the dispersion effects can be neglected at the location of the obstacle (in the so called hydraulic approximation) and the theory reduces to the scheme presented in Ref. [40]. In the second case the potential can be approximated by a  $\delta$  function and its action amounts to the matching condition of exact solutions at the point of its location. This last case has not been considered so far in this kind of problem and we shall discuss it here in detail. We will show that it makes it possible to realize asymptotically (i.e., at large time) a sonic horizon such as represented in Fig. 1.

The paper is organized as follows. In Sec. II we present the problem and the typical dynamical situation we aim at describing. In Sec. III we discuss the time-dependent analytical solutions of the flow in each of the characteristics regions of space identified in the previous section. In Sec. IV we briefly compare our results with the ones obtained in the case of a thick obstacle. In Sec. V we compare the analytical results with numerical simulations and propose an improvement of the analytical description. Finally we present our conclusions in Sec. VI.

## II. FORMULATION OF THE PROBLEM

In the so-called 1D-mean-field regime [43] the dynamics of the condensate is described by the Gross-Pitaevskii equation which governs the evolution of the wave function  $\psi(x,t)$ . Expressing densities in units of a reference density  $n_{\text{ref}}$ , energies, distances, and velocities in units of the corresponding chemical potential  $\mu_{\text{ref}}(n_{\text{ref}})$ , healing length  $\xi_{\text{ref}} = \hbar/(m\mu_{\text{ref}})^{1/2}$ , and speed of sound  $c_{\text{ref}} = \hbar/(m\xi_{\text{ref}})$ , one can write the Gross-Pitaevskii equation in the form

$$i\psi_t = -\frac{1}{2}\psi_{xx} + [U(x) + |\psi|^2]\psi. \quad (1)$$

The Gross-Pitaevskii equation is a sufficient ingredient for describing the generation of DSW in a BEC as shown by the comparisons between theory and experiments displayed in Refs. [44,45].

By means of the Madelung substitution

$$\psi(x,t) = \sqrt{n(x,t)} \exp\left[i \int^x u(x',t) dx'\right] e^{-i\mu t}, \quad (2)$$

the Gross-Pitaevskii equation can be cast into an hydrodynamic-like form for the density  $n(x,t)$  and the flow velocity  $u(x,t)$ :

$$\begin{aligned} n_t + (nu)_x &= 0, \\ u_t + uu_x + n_x + \left(\frac{n_x^2}{8n^2} - \frac{n_{xx}}{4n}\right)_x &= -U_x. \end{aligned} \quad (3)$$

We now briefly introduce the concept of Riemann invariant by considering the very simple example of the dispersionless limit of Eqs. (3). This case is not treated only for pedagogical purposes. At the boundary between the DSW and regions of flat profiles (where dispersion is indeed negligible) it will make it possible to match the description of the nonlinear wave in terms of elaborate Riemann variables [Eqs. (13) and (14)] with a simple description of the type specified by Eqs. (5), (6), and (7) [this matching will be achieved by means of Eqs. (23) and (25)].

The last term on the left hand-side of the last of Eqs. (3) is responsible for the dispersive character of the BEC wave. In the absence of potential, and in a regime where the effects of dispersion can be neglected, Eqs. (3) reduce to

$$n_t + (nu)_x = 0, \quad u_t + uu_x + n_x = 0. \quad (4)$$

These equations can be written in a more symmetric form by introducing the following Riemann invariants:

$$\lambda_{\pm}(x,t) = \frac{u(x,t)}{2} \pm \sqrt{n(x,t)}, \quad (5)$$

which evolve according to the equations [equivalent to (4)]

$$\partial_t \lambda_{\pm} + v_{\pm}(\lambda_+, \lambda_-) \partial_x \lambda_{\pm} = 0 \quad (6)$$

with

$$v_{\pm}(\lambda_+, \lambda_-) = \frac{1}{2}(3\lambda_{\pm} + \lambda_{\mp}). \quad (7)$$

We will encounter below other Riemann invariants which describe the DSW and obey equations similar to (6) and (7) [Eqs. (19) and (20)]. However, the dispersive nature of the shock will be there fully taken into account, in contrast to the simple approximations (4), (6), and (7).

Let us now present the initial velocity and density profile of the incident flow. We suppose that at initial time ( $t = 0$ ) a half-infinite pulse of BEC with a step-like distribution

$$\psi(x,t=0) = \begin{cases} \sqrt{n_0} \exp\{iu_0 x\} & \text{for } x < 0, \\ 0 & \text{for } x > 0 \end{cases} \quad (8)$$

collides with a repulsive  $\delta$  potential located at the origin of the coordinate system:

$$U(x) = \kappa \delta(x), \quad \kappa > 0. \quad (9)$$

In other words, the initial density and flow velocity are

$$n(x,t=0) = \begin{cases} n_0 & \text{for } x < 0, \\ 0 & \text{for } x > 0, \end{cases} \quad (10)$$

$$u(x,t=0) = \begin{cases} u_0(>0) & \text{for } x < 0, \\ 0 & \text{for } x > 0. \end{cases} \quad (11)$$

At later times, the typical situation we aim at describing is illustrated in Fig. 2 which represents the density distribution  $n(x,t)$

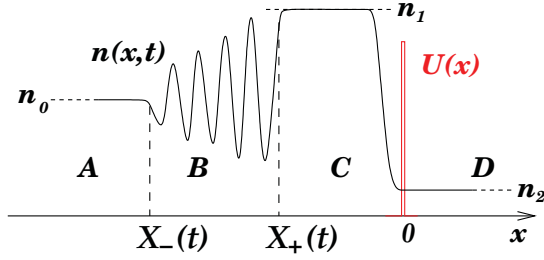


FIG. 2. (Color online) Sketch of the density profile  $n(x,t)$  at a given time  $t > 0$ . The flow is directed toward positive  $x$ . The regions denoted as A, B, C, and D are presented in the text. Points  $X_-(t)$  and  $X_+(t)$  are the small amplitude edge and soliton edge of the DSW (region B). The characteristic densities  $n_0$ ,  $n_1$ , and  $n_2$  are defined in the text [Eqs. (10), (24), and (26)].

at some fixed time  $t > 0$ . It corresponds to a flow initiated by the profile (10) and (11) in which a plateau develops upstream of the potential (region C) while a dispersive shock wave (region B) propagates away from the obstacle, in the negative direction. The flow just downstream from the obstacle forms a supersonic plateau (region D). The right edge of region D matches with a simple-wave solution (not shown in Fig. 2) which describes how the density vanishes at large  $x$ . In the present work we are not interested in the description of this part of the flow pattern. As one can see, the typical flow we consider can be subdivided in this case into several regions (denoted as A, B, C, and D in Fig. 2) with specific features in each region.

(1) In region A [ $x < X_-(t)$ ] we have the incoming flow  $\psi_A$  with the parameters (10) and (11). This flow can be considered as a boundary condition:

$$\begin{aligned} n_A(x,t) &= n_0, \\ u_A(x,t) &= u_0, \end{aligned} \quad x < X_-(t) \quad \text{for all } t > 0. \quad (12)$$

In this region there is no dispersion nor external potential and the analysis in terms of Riemann invariants (5) is trivially valid: the Riemann invariants are constant with  $\lambda_{\pm}^A = \frac{1}{2}u_0 \pm \sqrt{n_0}$ .

(2) In region B [ $X_-(t) < x < X_+(t)$ ] a dispersive shock wave takes place which can be described as a modulated periodic solution  $\psi_B(x,t)$  of Eqs. (1) and (3) with  $U(x) = 0$ . Such a solution can be written in the form (see, e.g., [40,46])

$$n_B(x,t) = \frac{1}{4}(\lambda_4 - \lambda_3 - \lambda_2 + \lambda_1)^2 + (\lambda_4 - \lambda_3)(\lambda_2 - \lambda_1) \times \text{sn}^2[\sqrt{(\lambda_4 - \lambda_2)(\lambda_3 - \lambda_1)}(x - Vt), m], \quad (13)$$

$$u_B(x,t) = V - \frac{C}{n_B(x,t)}, \quad (14)$$

where sn is the sine elliptic Jacobi function,

$$V = \frac{1}{2} \sum_{i=1}^4 \lambda_i, \quad m = \frac{(\lambda_2 - \lambda_1)(\lambda_4 - \lambda_3)}{(\lambda_4 - \lambda_2)(\lambda_3 - \lambda_1)} \quad (15)$$

and

$$C = \frac{1}{8}(-\lambda_1 - \lambda_2 + \lambda_3 + \lambda_4)(-\lambda_1 + \lambda_2 - \lambda_3 + \lambda_4) \times (\lambda_1 - \lambda_2 - \lambda_3 + \lambda_4). \quad (16)$$

In strictly periodic solutions the parameters  $\lambda_1 \leq \lambda_2 \leq \lambda_3 \leq \lambda_4$  are constant and they determine characteristics of the wave such as the amplitude of oscillations

$$a = (\lambda_2 - \lambda_1)(\lambda_4 - \lambda_3) \quad (17)$$

and the wavelength

$$L = \frac{2K(m)}{\sqrt{(\lambda_4 - \lambda_2)(\lambda_3 - \lambda_1)}}, \quad (18)$$

$K(m)$  being the complete elliptic integral of the first kind. In the limit  $m \rightarrow 0$  ( $\lambda_2 = \lambda_1$ ), (13) describes a small amplitude sinusoidal wave, and in the opposite case  $m \rightarrow 1$  ( $\lambda_2 = \lambda_3$ ) it describes a dark soliton. In the case of a slowly modulated dispersive shock wave such as occurring in region B, the  $\lambda$  are functions of  $x$  and  $t$  which vary weakly over one wavelength and one period. Their slow evolution is governed by the Whitham equations [46,47]

$$\frac{\partial \lambda_i}{\partial t} + v_i(\lambda_1, \lambda_2, \lambda_3, \lambda_4) \frac{\partial \lambda_i}{\partial x} = 0, \quad i = 1, 2, 3, 4. \quad (19)$$

Comparing with Eqs. (6) and (7) one sees that the  $\lambda_i$  are the Riemann invariants of the Whitham equations. The  $v_i$  are the characteristic velocities. Their  $\lambda_i$ 's dependence is much more complicated than the simple linear combinations appearing in (7); they can be expressed in terms of complete elliptic integrals of the first and the second kind [48,49]. One can use the following convenient formula for their computation [46,50]:

$$v_i = V - \frac{1}{2} \frac{L}{\partial L / \partial \lambda_i}, \quad i = 1, 2, 3, 4. \quad (20)$$

At  $x = X_-(t)$  we have the ‘‘small amplitude edge’’ of the dispersive shock wave [with  $\lambda_2(X_-(t), t) = \lambda_1(X_-(t), t)$ ] where the wave should satisfy the matching conditions with the flow in region A. This implies that the mean values of the density  $\bar{n}_B$  and the flow velocity  $\bar{u}_B$  coincide with  $n_0$  and  $u_0$ , respectively:

$$\bar{n}_B(X_-(t), t) = n_0, \quad \bar{u}_B(X_-(t), t) = u_0. \quad (21)$$

Since at the left edge of the DSW we have  $\lambda_2 = \lambda_1$ , the Whitham equations (19) for  $\lambda_3$  and  $\lambda_4$  can be shown to simplify to

$$\begin{aligned} \partial_t \lambda_3 + \frac{1}{2}(3\lambda_3 + \lambda_4) \partial_x \lambda_3 &= 0, \\ \partial_t \lambda_4 + \frac{1}{2}(\lambda_3 + 3\lambda_4) \partial_x \lambda_4 &= 0, \end{aligned} \quad (22)$$

and these equations can be identified with the Riemann form (6) and (7) of the dispersionless limit (4) of Eqs. (3) (without potential); that is, one has

$$\begin{aligned} \lambda_4(X_-(t), t) &= \lambda_+^A = \frac{1}{2}u_0 + \sqrt{n_0} \equiv \lambda_0, \\ \lambda_3(X_-(t), t) &= \lambda_-^A = \frac{1}{2}u_0 - \sqrt{n_0}. \end{aligned} \quad (23)$$

The other edge of the DSW occurs at  $x = X_+(t)$ . We denote it as the ‘‘soliton edge’’ because at this point the density oscillations are soliton-like:  $\lambda_2(X_+(t), t) = \lambda_3(X_+(t), t)$  (i.e.,  $m = 1$ ). The matching conditions at  $X_+$  read

$$\bar{n}_B(X_+(t), t) = n_1, \quad \bar{u}_B(X_+(t), t) = u_1, \quad (24)$$

where we suppose that  $X_+$  is located far enough from the origin in order that the stationary solution  $\psi_C$  in region B

reaches its asymptotic values  $n_c(x) \rightarrow n_1$ ,  $u_c(x) \rightarrow u_1$  when  $x \simeq X_+$  (i.e., in the formal limit  $x \rightarrow -\infty$  in region  $B$ , see below for more details). Since at the soliton edge  $\lambda_2 = \lambda_3$ , one can show as previously that the Whitham equations for  $\lambda_4$  and  $\lambda_1$  reduce to a form similar to (6) and (7) where  $\lambda_4$  plays the role of  $\lambda_+$  and  $\lambda_1$  plays the role of  $\lambda_-$ . Hence one has

$$\begin{aligned}\lambda_4(X_+(t), t) &= \lambda_+^c = \frac{1}{2}u_1 + \sqrt{n_1}, \\ \lambda_1(X_+(t), t) &= \lambda_-^c = \frac{1}{2}u_1 - \sqrt{n_1}.\end{aligned}\quad (25)$$

(3) Region  $C$  corresponds to a smooth and stationary solution  $\psi_c(x, t)$  of the Gross-Pitaevskii equation for  $X_+ < x < 0$  and region  $D$  to a smooth and stationary solution  $\psi_D$  for  $0 < x < X_{sw}$ . The flow at  $x > X_{sw}$  represents a simple wave solution (with small dispersive corrections) connecting region  $D$  with vacuum and is of no interest to us (this is the reason why we do not show the region  $x > X_{sw}$  in Fig. 2). In region  $D$  we have a uniform flow

$$\begin{aligned}n_D(x, t) &= n_2 = \text{const} \\ u_D(x, t) &= u_2 = \text{const}\end{aligned}\quad \text{for } 0 < x < X_{sw}.\quad (26)$$

Since the flow is stationary in both regions  $C$  and  $D$ , the parameters (24) and (26) must satisfy the condition of conservation of flux

$$n_1 u_1 = n_2 u_2, \quad (27)$$

and the Bernoulli law (constant value of the chemical potential  $\mu$ )

$$\frac{1}{2}u_1^2 + n_1 = \frac{1}{2}u_2^2 + n_2 = \mu. \quad (28)$$

One must also satisfy the condition of continuity of the wave function at  $x = 0$ ,

$$\psi_c(0, t) = \psi_D(0, t), \quad (29)$$

and the jump condition for the derivative of the wave function which follows from Eqs. (1) and (9)

$$\partial_x \psi_D(0, t) - \partial_x \psi_c(0, t) = 2\kappa \psi_c(0, t). \quad (30)$$

Thus, our task is to find the solution which satisfies all the above matching conditions [Eqs. (21), (24), (27)–(30)] and yields the parameters  $n_1$ ,  $u_1$ ,  $n_2$ ,  $u_2$ , and the positions  $X_{\pm}(t)$  of the edges of the DSW as functions of the incoming flow parameters  $n_0$ ,  $u_0$ , and of the potential strength  $\kappa$ . It is clear that such a solution does not exist for any choice of the parameters  $n_0$ ,  $u_0$ ,  $\kappa$ . For example, in the limit  $\kappa \rightarrow 0$  our system reduces to the well-known ‘‘dam problem’’ [46,47] which is described in the hydrodynamic approximation by a simple wave solution without formation of dispersive shock wave. Therefore our solution should be complemented by an explicit statement of its conditions of existence.

### III. SOLUTION OF THE PROBLEM

#### A. Dispersive shock wave (region $B$ )

As was indicated above, the DSW is described by four parameters  $\lambda_i$ ,  $i = 1, 2, 3, 4$ , which change slowly along the wave. We suppose that the DSW is detached from the obstacle and propagates upstream with the velocities  $V_{\pm}$  of the edge points  $X_{\pm}$ . The distance at which  $\psi_c$  reaches its asymptotic

value (with  $n_c \simeq n_1$ ,  $u_c \simeq u_1$ ) when one goes away from the origin is of order of the healing length in the region  $C$ , that is,  $\sim n_1^{-1/2}$ . Since this distance is much less than the (time increasing) length  $|X_+|$ , we can assume in good approximation that the formation of the plateau  $n_c \simeq n_1$ ,  $u_c \simeq u_1$  occurs instantaneously. Then the DSW can be described by a self-similar solution of the Whitham equations (19) and for the left-propagating DSW we get

$$\lambda_1 = \text{const}, \quad \lambda_3 = \text{const}, \quad \lambda_4 = \text{const}, \quad (31)$$

and

$$v_2(\lambda_1, \lambda_2(x/t), \lambda_3, \lambda_4) = \frac{x}{t}. \quad (32)$$

This is the so-called Gurevich-Pitaevskii problem introduced into the theory of DSW in Ref. [51] and used for description of internal waves generated by the flow of water past an uneven bottom in [52,53] (see also [40] and references therein).

When  $n_1$  and  $u_1$  are found, the values of the constants  $\lambda_1$ ,  $\lambda_3$ , and  $\lambda_4$  can be determined from Eqs. (23) and (25), whereas Eqs. (20) and (32) determine  $\lambda_2$  as a function of  $x/t$ :

$$\begin{aligned}v_2(\lambda_1, \lambda_2, \lambda_3, \lambda_4) &= \frac{1}{2} \sum_i \lambda_i + \frac{(\lambda_3 - \lambda_2)(\lambda_2 - \lambda_1)\mathbf{K}(m)}{(\lambda_3 - \lambda_2)\mathbf{K}(m) - (\lambda_3 - \lambda_1)\mathbf{E}(m)} = \frac{x}{t}.\end{aligned}\quad (33)$$

The plots of  $\lambda_i$ ,  $i = 1, 2, 3, 4$ , as functions of  $x/t$  are displayed in Fig. 3. The left edge of the DSW moves with velocity

$$\begin{aligned}V_- &\equiv \frac{X_-}{t} = v_2(\lambda_1, \lambda_1, \lambda_3, \lambda_4) \\ &= \frac{1}{2}(2\lambda_1 + \lambda_3 + \lambda_4) + \frac{2(\lambda_3 - \lambda_1)(\lambda_4 - \lambda_1)}{2\lambda_1 - \lambda_3 - \lambda_4},\end{aligned}\quad (34)$$

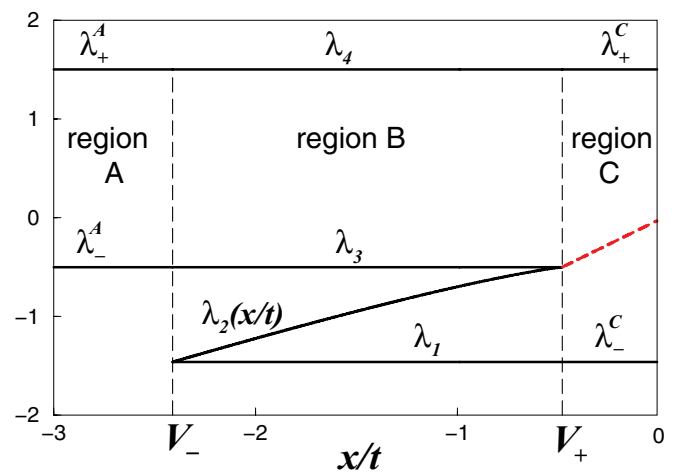


FIG. 3. (Color online) The Riemann invariants plotted as functions of the self-similar variable  $x/t$  in regions  $A$ ,  $B$ , and  $C$ . In region  $C$  the (red) dashed line (not considered in Sec. III) corresponds to the soliton train with  $\lambda_2 = \lambda_3 = x/t - u_1/2$  discussed in Sec. V [Eq. (86)]. The figure is drawn for the situation studied in Sec. V, with  $n_0 = 1$ ,  $u_0 = 1$ , and  $\kappa = 5.2$ . The corresponding velocities of the edges of the DSW (region  $B$ ) are  $V_- = -2.4$  and  $V_+ = -0.48$ .

and the right edge moves with velocity

$$V_+ \equiv \frac{X_+}{t} = v_2(\lambda_1, \lambda_3, \lambda_3, \lambda_4) = \frac{1}{2}(\lambda_1 + 2\lambda_3 + \lambda_4). \quad (35)$$

For finding  $n_1, u_1$ , and, hence,  $\lambda_1$ , we have to turn to the solution of the Gross-Pitaevskii equation in region  $C$  and its matching with the solution in region  $D$ .

### B. Flow across the $\delta$ potential (regions $C$ and $D$ )

In regions  $C$  and  $D$  the flow is stationary,  $\psi(x, t) = e^{-i\mu t} \varphi(x)$ , so that the Gross-Pitaevskii equation reduces to

$$-\frac{1}{2}\varphi_{xx} + |\varphi|^2\varphi + \kappa\delta(x)\varphi = \left(\frac{1}{2}u_1^2 + n_1\right)\varphi. \quad (36)$$

It is convenient to introduce temporarily the variables

$$\begin{aligned} \varphi &= \sqrt{n_1}\phi, & u_1 &= \sqrt{n_1}M_c, \\ y &= \sqrt{n_1}x, & \tilde{\kappa} &= \frac{\kappa}{\sqrt{n_1}}, \end{aligned} \quad (37)$$

$M_c$  being the asymptotic (formally at  $x \rightarrow -\infty$ ) Mach number of the flow in region  $C$ . Then Eq. (36) takes the form

$$-\frac{1}{2}\phi_{yy} + |\phi|^2\phi + \tilde{\kappa}\delta(y)\phi = \left(\frac{1}{2}M_c^2 + 1\right)\phi. \quad (38)$$

From conservation of the flow (27) we get

$$\frac{u_2}{u_1} = \frac{n_1}{n_2} \equiv \eta, \quad (39)$$

and  $\eta$  can be found as a function of  $M_c = u_1/\sqrt{n_1} < 1$  with the use of Eq. (28) or

$$\frac{M_c^2}{2}\eta^3 - \left(1 + \frac{M_c^2}{2}\right)\eta + 1 = 0. \quad (40)$$

The relevant solution ( $\eta > 1$ ) of this equation is given by

$$\eta = \frac{1}{2} \left( \sqrt{1 + \frac{8}{M_c^2}} - 1 \right). \quad (41)$$

We look for a solution of Eq. (38) of the form

$$\phi(y) = e^{iyM_c} \{ \cos\theta \tanh[(y - y_0)\cos\theta] - i \sin\theta \} \quad (42)$$

for  $y < 0$  and

$$\phi(y) = -\frac{1}{\eta} e^{i(y\eta M_c + \gamma)} \quad (43)$$

for  $y > 0$ . In the above expressions (42) and (43) we have  $u_2/\sqrt{n_1} = \eta M_c$  and  $\sin\theta = M_c$ . This solution has been first identified in Ref. [35]. The flow upstream from the obstacle corresponds to a portion of a dark soliton which is attached at  $y = 0$  to a downstream supersonic flow. The condition of continuity of the function  $\phi(y)$  at  $y = 0$  [see (29)] gives

$$\sin\gamma = \sqrt{\eta} \sin\theta, \quad \cos\gamma = \sqrt{\eta} \tanh(y_0 \cos\theta), \quad (44)$$

from which we get

$$\tanh(y_0 \cos\theta) = \sqrt{\frac{1 - \eta M_c^2}{\eta(1 - M_c^2)}}. \quad (45)$$

The condition (30) takes the form

$$\phi_y(0^+) - \phi_y(0^-) = 2\tilde{\kappa}\phi(0). \quad (46)$$

Substitution of expressions (42) and (43) in this relation gives after some algebra with the use of Eqs. (44) and (45) the equation

$$(\eta - 1)\sqrt{\frac{1}{\eta^2} - M_c^2} = 2\tilde{\kappa}. \quad (47)$$

Elimination of  $\eta$  with the help of Eqs. (41) yields

$$\tilde{\kappa} = F(M_c), \quad \text{i.e.,} \quad \kappa = \sqrt{n_1}F(M_c), \quad (48)$$

where

$$F(M_c) = \frac{M_c}{8} \left( \sqrt{1 + \frac{8}{M_c^2}} - 3 \right)^{3/2}. \quad (49)$$

Hence, according to (37)

$$u_1 = \sqrt{n_1}M_c = \frac{\kappa M_c}{F(M_c)}. \quad (50)$$

Then Eqs. (39) and (41) yield the expressions for  $n_2$  and  $u_2$ :

$$n_2 = \frac{n_1}{\eta} = \frac{\kappa^2 M_c^2}{4F^2(M_c)} \left( \sqrt{1 + \frac{8}{M_c^2}} + 1 \right), \quad (51)$$

$$u_2 = u_1\eta = \frac{\kappa M_c}{2F(M_c)} \left( \sqrt{1 + \frac{8}{M_c^2}} - 1 \right). \quad (52)$$

We thus have obtained the parameters  $n_1, u_1, n_2, u_2$  as functions of  $\kappa$  and  $M_c$ . We now have to relate  $M_c$  to the physical parameters  $n_0$  and  $u_0$  which describe the incoming flow.

### C. The global solution

To get the global solution, we use the relation  $\lambda_+^A = \lambda_4 = \lambda_+^C$  [see Eqs. (23) and (25) and Fig. 3] and (48) and (50) to obtain

$$\lambda_0 \equiv \frac{1}{2}u_0 + \sqrt{n_0} = \frac{1}{2}u_1 + \sqrt{n_1} = \frac{\kappa}{F(M_c)} \left( 1 + \frac{M_c}{2} \right). \quad (53)$$

As a result, all expressions can be written in a parametric form with  $M_c$  playing the role of the parameter. From (53) we get

$$\kappa(\lambda_0, M_c) = \lambda_0 \frac{F(M_c)}{1 + M_c/2}, \quad (54)$$

which determines  $M_c$  as a function of  $\kappa$  and  $\lambda_0$ . Substitution of this expression into (48)–(50) yields

$$n_1(\lambda_0, M_c) = \frac{\lambda_0^2}{(1 + M_c/2)^2}, \quad u_1(\lambda_0, M_c) = \frac{\lambda_0 M_c}{1 + M_c/2}, \quad (55)$$

$$n_2(\lambda_0, M_c) = \frac{\lambda_0^2 M_c^2}{(2 + M_c)^2} \left( \sqrt{1 + \frac{8}{M_c^2}} - 1 \right), \quad (56)$$

$$u_2(\lambda_0, M_c) = \frac{\lambda_0 M_c}{2 + M_c} \left( \sqrt{1 + \frac{8}{M_c^2}} + 1 \right). \quad (57)$$

In combination with (54), formulas (55)–(57) determine—in a parametric form—the dependence of  $n_1, u_1, n_2, u_2$  on  $\kappa$  and  $\lambda_0 = \frac{1}{2}u_0 + \sqrt{n_0}$ . These formulas represent an important step in our study since they determine the overall structure of the flow ( $n_1, u_1, n_2$ , and  $u_2$ ) as a function of the initial parameters

characterizing the incident beam ( $n_0$  and  $u_0$ ) and the obstacle ( $\kappa$ ) with which it collides.

Actually, the overall structure of the flow is fully characterized only once the locations  $X_-(t)$  and  $X_+(t)$  of the boundaries between the different zones are known (cf. Fig. 2). According to our self-similarity hypothesis  $X_{\pm}(t) = V_{\pm}t$ , where  $V_{\pm}$  are the time-independent velocities of the boundaries. Now that  $n_1$  and  $u_1$  are found,  $V_+$  and  $V_-$  are simply determined as follows. One first can get [from Eqs. (23) and (25)] the expressions for the three Riemann invariants which remain constant in the region of the DSW

$$\begin{aligned}\lambda_1 &= -\lambda_0 \frac{2 - M_c}{2 + M_c}, \\ \lambda_3 &= \frac{1}{2}u_0 - \sqrt{n_0} \\ \lambda_4 &= \lambda_0 = \frac{1}{2}u_0 + \sqrt{n_0}\end{aligned}\quad (58)$$

Then, substitution of formulas (58) into Eqs. (34) and (35) yields the desired expressions of the velocities  $V_-$  and  $V_+$  of the edge points of the shock wave. In particular, it is interesting to realize [cf. Eq. (61)] that the velocity  $V_-$  of the small amplitude edge  $X_-$  of the DSW corresponds to the group velocity of linear excitations in region A of the system with wavelength  $L(X_-)$ , where  $L$  is the (position-dependent) wavelength of the nonlinear oscillations (13). This is obtained by noticing that the explicit formula (34) and the expressions (58) of the Riemann invariants makes it possible to write  $V_-$  under the form

$$\begin{aligned}V_- &= u_0 + 2\sqrt{n_0} \frac{1 + M_c/2}{M_c - 2 - 2M_0} \\ &\times \left[ 1 + 2 \frac{(2 + M_0)(M_0 - M_c)}{(1 + M_c/2)^2} \right],\end{aligned}\quad (59)$$

where  $M_0 = u_0/\sqrt{n_0}$ . Similarly, when  $\lambda_1 = \lambda_2$ , the expression (18) for  $L$  reduces to

$$\begin{aligned}L(X_-) &= \frac{\pi}{\sqrt{(\lambda_4 - \lambda_1)(\lambda_3 - \lambda_1)}} \\ &= \frac{\pi}{\sqrt{n_0}} \frac{(1 + M_c/2)}{\sqrt{(M_0 + 2)(M_0 - M_c)}}.\end{aligned}\quad (60)$$

Defining  $k = 2\pi\sqrt{n_0}/L(X_-)$  as the dimensionless wave vector at the small amplitude edge of the DSW, it is a simple exercise to show that using Eq. (60) one can rewrite (59) under the form

$$V_- = u_0 - c_0 \frac{1 + k^2/2}{\sqrt{1 + k^2/4}},\quad (61)$$

which is the group velocity of excitations whose dispersion relation is given by  $\omega(k) = u_0k - c_0k\sqrt{1 + k^2/4}$ , where  $c_0 = \sqrt{n_0}$  is the speed of sound in a uniform system at rest with density  $n_0$ . This dispersion relation corresponds to (left propagating) linear elementary excitations in a BEC with constant density  $n_0$  and constant velocity  $u_0$ . Relation (61) is very natural since  $V_-$  is the velocity of the small amplitude edge  $X_-$  at which the DSW is linear: the linear front of a wave packet should propagate with the appropriate group velocity. This is a generic feature of the small amplitude edge of a DSW, as proven on general grounds in Ref. [54]. Relation (61)

nonetheless constitutes a nontrivial check of the validity of our description since the connection between  $V_-$  and  $L(X_-)$  is not straightforward.

As for the soliton edge of the DSW, we obtain from Eqs. (35) and (58)

$$V_+ = \frac{u_0(1 + M_c) - 2\sqrt{n_0}}{2 + M_c}.\quad (62)$$

This is the velocity of the edge soliton whose amplitude is equal to

$$a = (\lambda_3 - \lambda_1)(\lambda_4 - \lambda_3) = \frac{4\sqrt{n_0}(u_0 - M_c\sqrt{n_0})}{2 + M_c}.\quad (63)$$

Note that our approach not only determines the gross features of the flow (those which are depicted in Fig. 2:  $u_1$ ,  $n_1$ ,  $u_2$ ,  $n_2$ , and  $X_{\pm}$ ) but also yields a precise prediction for the density profile in the region of the obstacle and of the DSW. In the region of the obstacle the order parameter is determined by Eqs. (42) and (43). In the region of the DSW, the velocity and the density profile are determined by Eqs. (13) and (14) which need the input of the  $\lambda_i$  [Eqs. (32) and (58)]. These predictions will be tested against numerical simulations in Sec. V.

The solution found here is based on two assumptions: (i) that the discontinuity  $n_1 > n_0$  arises after collision of the BEC pulse with the obstacle. This is equivalent to the condition  $a > 0$  or

$$\frac{u_0}{\sqrt{n_0}} > M_c,\quad (64)$$

and (ii) that the DSW is detached from the obstacle, that is,  $V_+ < 0$  or

$$\frac{u_0}{\sqrt{n_0}} < \frac{2}{1 + M_c}.\quad (65)$$

If the density  $n_0$  is fixed, then Eq. (64) gives the lower velocity  $u_0$  below which—and Eq. (65) gives the upper velocity above which—the solution we are interested in disappears. These critical values of  $u_0$  are functions of the incoming density  $n_0$  and of the potential strength  $\kappa$  determined by the equations

$$F\left(\frac{u_0}{\sqrt{n_0}}\right) = \frac{\kappa}{\sqrt{n_0}} \quad (\text{lower boundary})\quad (66)$$

and

$$\frac{u_0}{\sqrt{n_0}} F\left(2\frac{\sqrt{n_0}}{u_0} - 1\right) = \frac{\kappa}{\sqrt{n_0}} \quad (\text{upper boundary}),\quad (67)$$

where we recall that function  $F$  is defined by (49). These two curves are plotted in Fig. 4.

For small  $\kappa/\sqrt{n_0}$  we get the series expansions:

$$\frac{u_0}{\sqrt{n_0}} \simeq 1 - \frac{3}{2}\left(\frac{\kappa}{\sqrt{n_0}}\right)^{2/3} \quad (\text{lower boundary})\quad (68)$$

and

$$\frac{u_0}{\sqrt{n_0}} \simeq 1 + \frac{3}{4}\left(\frac{\kappa}{\sqrt{n_0}}\right)^{2/3} \quad (\text{upper boundary}).\quad (69)$$

In the opposite limit of large  $\kappa/\sqrt{n_0}$  we get

$$\frac{u_0}{\sqrt{n_0}} \simeq \frac{1}{2\sqrt{2}}\left(\frac{\kappa}{\sqrt{n_0}}\right)^{-2} \quad (\text{lower boundary})\quad (70)$$

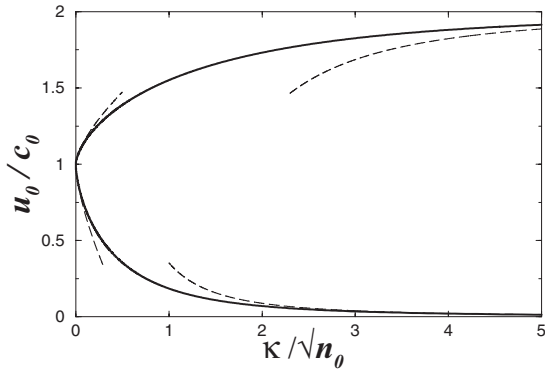


FIG. 4. Boundaries of the region of parameters for which the DSW is expelled upstream from the obstacle. The vertical axis is the speed of the incident beam in units of the speed of sound  $c_0 = \sqrt{n_0}$ . The horizontal axis is the dimensionless strength  $\kappa/\sqrt{n_0}$  of the  $\delta$  potential. The DSW is expelled from the region of the obstacle when the point representative of the system lies between the two solid curves which correspond to Eqs. (66) and (67). The dashed curves are the approximate boundaries (68), (69) (valid when  $\kappa/\sqrt{n_0} \ll 1$ ), (70), and (71) (valid when  $\kappa/\sqrt{n_0} \gg 1$ ).

and

$$\frac{u_0}{\sqrt{n_0}} \simeq 2 - 2\sqrt{2} \left( \frac{\kappa}{\sqrt{n_0}} \right)^{-2} \quad (\text{upper boundary}). \quad (71)$$

We emphasize here that Eqs. (66) and (67) are important results of our study because they determine the region of parameters for which our analytical solution exists, that is, for which (i) the DSW is expelled upstream from the obstacle and (ii) the flow forms in vicinity of the obstacle a sonic horizon such as schematically represented in Fig. 1.

In this line it is important to notice that the above approach is not applicable for positive values of the soliton edge velocity  $V_+ > 0$ , that is, when the soliton edge of the DSW is attached to the obstacle. This is different from what happens in the case of thick obstacles [40] where the existence of a characteristic length  $l$  of the potential representing the obstacle plays a crucial role. Since in this case  $l$  is large compared with the wavelength of the (possibly attached) DSW, the regions of DSW and of the “hydraulic solution” in vicinity of the obstacle are well separated and one can safely assume formation of a plateau at the left boundary of the region of the hydraulic solution. In the present case of a  $\delta$  potential such a plateau forms at a distance of the same order of magnitude as the DSW wavelength and, hence, in the case where the DSW is attached to the obstacle the solution of region C (see Fig. 2) completely disappears and the formulas derived above lose their meaning.

#### IV. COMPARISON WITH THE FLOW PAST A WIDE PENETRABLE BARRIER

In this section we briefly compare the results we obtained for a thin potential with those obtained in Ref. [40] for a wide and smooth potential  $U(x)$  which takes its maximal value at  $x = 0$ ,

$$U_m = \max\{U(x)\} = U(0), \quad (72)$$

and differs from zero only inside the region

$$-l \lesssim x \lesssim l. \quad (73)$$

If  $l$  and all lengths characteristic of the potential are much larger than the healing length of the condensate, the transition from an upstream subsonic flow to a downstream supersonic one is described by the so-called “transcritical flow” [40]. It is obtained for an incoming velocity  $u_0 \in [u_-, u_+]$ , where the critical velocities  $u_{\pm}$  are the roots of the equation

$$\frac{1}{2}u^2 - \frac{3}{2}u^{2/3} + 1 = U_m \quad (74)$$

(to simplify the notation, in this section we assume  $n_{\text{ref}} = n_0$ ). If  $U_m \ll 1$ , the critical velocities are given by the series expansions

$$u_{\pm} \approx 1 \pm \sqrt{\frac{3U_m}{2}}. \quad (75)$$

Flow velocities  $u_{1,2}$  at the boundaries of the hydraulic region are roots of the equation

$$\frac{u^2}{2} + \left( \frac{u_0 - u}{2} + 1 \right)^2 - \frac{3}{2} \left[ u \left( \frac{u_0 - u}{2} + 1 \right) \right]^{2/3} = U_m. \quad (76)$$

The smaller root corresponds to the upstream velocity  $u_1$  and the larger one to the downstream velocity  $u_2$ . If  $U_m \ll 1$  we get

$$\begin{aligned} u_1 &= 1 + \frac{1}{3}(u_0 - 1) - \sqrt{\frac{2U_m}{3}}, \\ u_2 &= 1 + \frac{1}{3}(u_0 - 1) + \sqrt{\frac{2U_m}{3}}. \end{aligned} \quad (77)$$

The DSWs can be attached to the transcritical flow as accounted for in detail in [40]. In our initial value problem, with a wave packet incoming from the left infinity, there can be no downstream DSW. However, an upstream DSW exists. It is detached from the obstacle only if the condition  $u_0 < 2 - u_1$  is fulfilled. Thus, the solution we are interested in, with a DSW expelled upstream from the region of the obstacle, corresponds to a region in the plane  $(U_m, u_0)$  where

$$u_- < u_0 < 2 - u_1. \quad (78)$$

This determines the parameters of the flow and of the potential leading to the formation of an acoustic analog of a black hole in the flow of a condensate past a thick obstacle. If  $U_m \ll 1$ , then inequalities (78) take the form

$$1 - \sqrt{\frac{3U_m}{2}} < u_0 < 1 + \sqrt{\frac{3U_m}{8}}. \quad (79)$$

The whole region (78) is shown in Fig. 5 which is the thick obstacle analog of Fig. 4.

#### V. COMPARISON WITH NUMERICAL SIMULATIONS

Our analytical theory is based on the assumption that the stationary flow with a plateau in region C is formed instantaneously after collision of the condensate with the obstacle. This assumption justifies the application of the self-similar solution [characterized by formulas (31) and (32)]

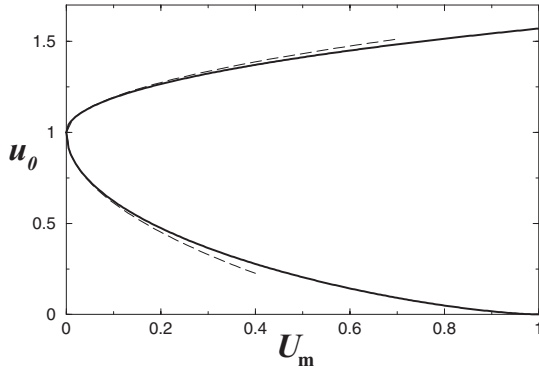


FIG. 5. Boundaries of the region (78) for which the hydraulic solution exists and the upstream DSW is detached from a thick and smooth obstacle (here we use units such that  $n_0 = 1$ ). The dashed lines correspond to the approximations (79) which are valid when  $U_m \ll 1$ .

which only depends on the variable  $x/t$ . However, in practice (i) any initial wave packet has—contrarily to our simplified initial flow (8)—a finite region of transition from a constant plateau density to vacuum, and (ii) the stationary solution in region  $C$  forms in a period of time negligibly small compared with the asymptotic values of time under consideration, but nonetheless finite, and this may induce some noticeable effects. Therefore we performed numerical simulations for determining the limitations of our analytical approach.

In our numerics the incident condensate wave packet was represented by the following initial density distribution:

$$n(x, t = 0) = n_0 \left[ \frac{1 - \tanh(x/\Delta)}{2} \right]^4. \quad (80)$$

According to the prescription of Sec. II we take here  $n_{\text{ref}} = n_0$ , so that  $n_0 = 1$  henceforth. The velocity of the incident flow is taken to be  $u_0 = 1$  (i.e.,  $u_0 = c_0 = c_{\text{ref}}$ ). We consider three different cases with different thicknesses  $\Delta$  of the incident front of the wave packet:  $\Delta = 20, 10$ , and  $5$  (in units of  $\xi_0 = \xi_{\text{ref}}$ ). The obstacle is modeled by a Gaussian potential

$$U(x) = U_0 \exp\{-x^2/\sigma^2\} \quad (81)$$

with  $U_0 = 4$  and  $\sigma = 0.5$  (i.e., the size of the obstacle is less than the healing length).

The results of the numerical evolution of the flow after a time  $t = 500$  are shown in Fig. 6, where the different numerical curves correspond to different values of  $\Delta$ . The potential (81) deviates significantly from a  $\delta$  potential: we have here  $\sigma = 0.5$  which is too large for using the natural prescription for defining, starting from (81), an equivalent  $\delta$  potential of the form (9) by  $\kappa = \int U(x)dx = U_0\sigma\sqrt{\pi} = 3.5$ . This prescription would be accurate only in the limit  $\sigma \ll 1$ . The value  $\kappa = 5.2$  used in the analytical procedure results from a fit of the numerically obtained density of the plateau ( $n_1 = 2.192$ ); then all the other parameters of the flow are determined by the analytical formulas. That this procedure is legitimate is confirmed by the very good description of the upstream velocity  $u_1$  in region  $C$  and of the density  $n_2$  and velocity  $u_2$  in the supersonic downstream region  $D$ : one obtains analytically  $u_1 = 0.0390, n_2 = 0.0412$ , and  $u_2 = 2.075$ , whereas one finds

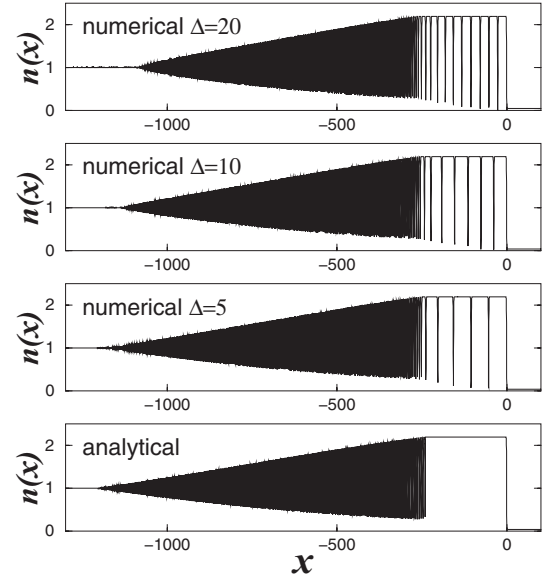


FIG. 6. Density profiles at  $t = 500$ . The three upper panels present the results of numerical simulations performed in the case where the obstacle is represented by the Gaussian potential (81) and the incident beam by (80) with  $\Delta = 20, 10$ , and  $5$ . The lower panel is the analytical result corresponding to a point-like obstacle (9) and a step-like incident beam (10) and (11), that is,  $\Delta = 0$ .

numerically  $u_1 = 0.0388, n_2 = 0.0410$ , and  $u_2 = 2.075$  (see also Fig. 7).

We checked that the natural prescription  $\kappa = U_0\sigma\sqrt{\pi}$  yields a very good agreement of the analytical and of the numerical approaches for low values of  $\sigma$ . For instance, when  $U_0 = 4$  and  $\sigma = 0.1$  the natural prescription yields  $\kappa = 0.71$  and for this value of  $\kappa$  one obtains analytically  $n_1 = 1.658$ , whereas one finds numerically  $n_1 = 1.6703$ . In this case perfect agreement with the numerical values of  $n_1, n_2, u_1$ , and  $u_2$  is found by using an effective  $\kappa = 0.7365$ , close to the natural prescription. However, for reducing the numerical effort we

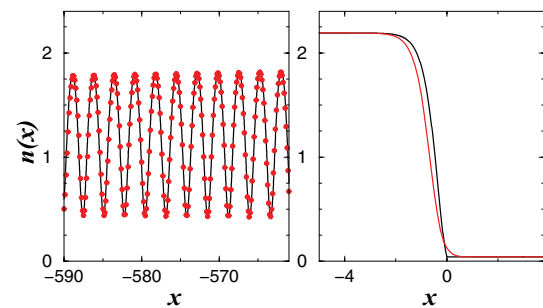


FIG. 7. (Color online) Density profiles at  $t = 500$ . These plots are enlargements of specific parts of the two lower plots of Fig. 6. The left plot concerns a part of the DSW ( $-590 < x < -560$ ), and the right one concentrates on the region of the obstacle. In both the right and left plots the black solid line corresponds to the analytical density profile. In the right plot the red solid line is the numerical density computed in the case  $\Delta = 5$ . The numerical profile is represented by red points in the left plot, because it would be indistinguishable from the analytical result if represented with a solid line.

performed extensive simulations only in the case  $\sigma = 0.5$ . The efficiency of the effective  $\delta$  barrier for representing a potential of the form (81) even though  $\sigma$  is not very small is a positive test of the robustness of our analytical description of the system.

We note that the theory predicts the conservation of the Riemann invariant

$$\lambda_{\pm}^A (= \lambda_0 = 1.5) = \lambda_{\pm}^C = u_1/2 + \sqrt{n_1} \quad (82)$$

across the DSW (cf. Fig. 3) and that this is fulfilled with very good accuracy in the numerical simulations. The positions  $X_{\pm}(t)$  of the edges of the DSW are also in good agreement with the theoretical prediction. Because of the scale used on the  $x$  axis of Fig. 6, one could think that the density is discontinuous around  $x = 0$ . This is not the case, and furthermore one can verify that in this region the analytical and numerical density profiles are very similar, as shown in Fig. 7 (right plot). Also inside the DSW, the nonlinear oscillations are very well described by the analytical approach (Fig. 7, left plot).

Hence we can legitimately state that the hypothesis of rapid formation of the DSW which, as already explained, is at the heart of our assumption of self-similarity, is validated by the comparison with numerical simulations. This makes it possible to bypass the delicate and interesting question of the short-time dynamics which is discussed for instance in Ref. [42]. However, our numerical simulations reveal a peculiar feature of the flow, namely a train of dark solitons is observed along the plateau in region C (cf. Fig. 6, upper panels). As it is clear from the figure, the number of solitons in the plateau decreases with  $\Delta$  and the appearance of a train of solitons is thus an effect of the finite width of the front of the initial wave packet. These solitons are generated at the initial stage of evolution and their precise characteristics depend on the details of the initial density distribution. We note that the number of solitons in the train is several orders of magnitude lower than the number of nonlinear oscillations in the DSW (see Fig. 6), that is, the existence of this train of solitons is a minor effect in our asymptotic description of the flow. Nonetheless, in any experiment the incident wave packet will not be infinitely sharp and the resulting train of solitons should be easily observed. It is therefore worth spending some time discussing its properties.

The periodic solution (13) and (14) describes a train of solitons if one considers a situation where  $\lambda_2 = \lambda_3$  while the other Riemann invariants ( $\lambda_1$  and  $\lambda_4$ ) remain constant. Here one has

$$\lambda_1 = -\lambda_0 \frac{2 - M_c}{2 + M_c}, \quad \lambda_4 = \lambda_0. \quad (83)$$

The velocity  $V$  and minimal density  $n_{\min}$  of one of the solitons of the train can be expressed as functions of the coinciding Riemann invariants  $\lambda_2(x, t) = \lambda_3(x, t)$ :

$$V = \frac{1}{2}(\lambda_1 + 2\lambda_3 + \lambda_4) = \frac{u_1}{2} + \lambda_3 \quad (84)$$

and

$$\begin{aligned} n_{\min} &= \frac{1}{2}(\lambda_1 + \lambda_4)^2 - \lambda_3(\lambda_1 + \lambda_4 - \lambda_3) \\ &= \frac{7}{4}u_1^2 - u_1V + V^2, \end{aligned} \quad (85)$$

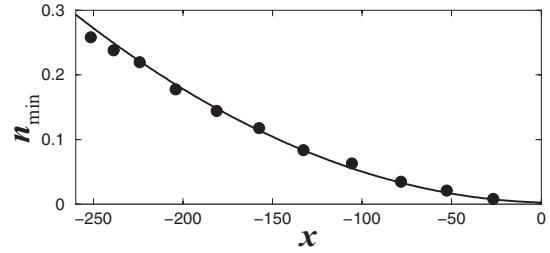


FIG. 8. The thick solid line represents the analytical prediction (87) for the positions of the points of minimal density of the soliton train at time  $t = 500$ . The value  $u_1 = 0.039$  was used in the plot of Eq. (87) [see discussion below Eq. (85)]. The dots show the same quantity obtained from the density profile  $n(x, t = 500)$  computed numerically in the case  $\Delta = 20$  (see Fig. 6, upper panel).

where  $u_1$  is given by Eq. (55),  $M_c$  being determined as a function of  $\kappa$  and  $\lambda_0$  by Eq. (54). In the present case ( $n_0 = 1$ ,  $u_0 = 1$ , and  $\kappa = 5.2$ ) one gets  $u_1 = 0.039$ . In accordance with the general spirit of our approach, we again assume self-similarity of the solution, that is, the locations of the solitons are given by an equation of the form  $x = Vt$ . The corresponding values of

$$\lambda_2 = \lambda_3 = \frac{x}{t} - \frac{u_1}{2} \quad (86)$$

are shown in Fig. 3 as a (red online) dashed line attached to the soliton edge of the DSW [55]. Note that (86) corresponds to the solution (32) of the Whitham equation in the soliton limit where  $\lambda_2(x/t) = \lambda_3(x/t)$ .

Then, elimination of  $V$  from (85) yields the following relation:

$$n_{\min} = \frac{7}{4}u_1^2 - u_1 \frac{x}{t} + \left(\frac{x}{t}\right)^2 \quad (87)$$

between two easily measurable parameters: the minimal density  $n_{\min}$  of a soliton and its coordinate  $x$  at time  $t$ . The very good agreement of this analytical prediction with the numerical results is illustrated in Fig. 8 where the solid line represents the curve (87), whereas the dots show the minimal density at the position of the solitons as observed in Fig. 6, upper panel (in the case where  $\Delta = 20$ ).

Hence, although the detailed description of all the features of the soliton train—depending of the precise shape of the incident front of the wave packet and of the potential—is beyond the scope of our approach, we still can get some insight on the loci of the density minima by assuming a kind of self-similarity which relies on the fact—confirmed by inspection of the numerical simulations—that the train is formed in a very short period, at the initial stage of the collision between the condensate and the obstacle. It then evolves according to the solitonic limit of Whitham equations.

## VI. CONCLUSIONS

In the present work we studied the flow of a Bose-Einstein beam incident onto an obstacle in a regime where a structure forms similar to the supersonic expansion obtained in a Laval

nozzle. For an appropriate choice of incident flow and of potential modeling the obstacle we showed that, at large time, an acoustic horizon is created around the obstacle. Its formation is accompanied by a release of energy in the form of a dispersive shock wave whose characteristics were studied in detail. This made it possible to precisely determine the condition of formation of the structure studied in the present work (see Fig. 4).

The analytical description has been sustained by numerical simulations which confirmed our analysis. The numerics however revealed an interesting and unexpected feature: the ejection of the DSW from the region of the horizon is typically accompanied by a train of dark solitons which are only slowly expelled from the obstacle. We argued that this train of solitons is formed in the initial stage of collision of the Bose-Einstein beam with the obstacle and that its detailed characteristics depend on the precise shape of the incident beam and of the obstacle potential. We also showed that one of its important features can be described analytically (namely the line of location of the density minima), precisely because this train is formed in an early stage.

The existence of this history-dependent train of solitons is due to the specific dispersive and nonlinear wave mechanics describing the Bose-Einstein condensate. It remains to investigate whether this train of solitons does or does not hinder the experimental observation of sonic analog of Hawking radiation.

#### ACKNOWLEDGMENTS

We would like to warmly thank I. Carusotto with whom we first discussed and observed numerically the formation of the dispersive shock structure presented in this work, who provided us with his numerical code and made judicious remarks on the manuscript. A.M.K. thanks LPTMS (Université Paris Sud and CNRS), where this work was done, for kind hospitality and financial support. This work was supported by the IFRAF Institute, by Grant ANR-08-BLAN-0165-01 and by RFBR (Grant 09-02-00499). The research presented in this work was partly performed in the framework of the associated European laboratory “Theoretical Physics and Condensed Matter” (ENS-LANDAU).

- 
- [1] L. D. Landau, *J. Phys. (USSR)* **5**, 71 (1940); **11**, 91 (1947), reprinted in I. M. Khalatnikov, *An Introduction to the Theory of Superfluidity* (Perseus Publishing, Cambridge, 2000).
  - [2] J. Wilks, *The Properties of Liquid and Solid Helium*, International Series of Monographs on Physics (Clarendon, Oxford, 1967).
  - [3] R. P. Feynman, in *Progress in Low Temperature Physics*, edited by C. J. Gorter (North-Holland, Amsterdam, 1955), Vol. I, p. 17.
  - [4] T. Winiecki, J. F. McCann, and C. S. Adams, *Phys. Rev. Lett.* **82**, 5186 (1999).
  - [5] I. Carusotto, S. X. Hu, L. A. Collins, and A. Smerzi, *Phys. Rev. Lett.* **97**, 260403 (2006).
  - [6] Yu. G. Gladush, G. A. El, A. Gammal, and A. M. Kamchatnov, *Phys. Rev. A* **75**, 033619 (2007).
  - [7] Yu. G. Gladush, L. A. Smirnov, and A. M. Kamchatnov, *J. Phys. B* **41**, 165301 (2008).
  - [8] C. Raman, M. Kohl, R. Onofrio, D.S. Durfee, C.E. Kuklewicz, Z. Hadzibabic, and W. Ketterle, *Phys. Rev. Lett.* **83**, 2502 (1999).
  - [9] A. Amo *et al.*, *Nat. Phys.* **5**, 805 (2009).
  - [10] T. Frisch, Y. Pomeau, and S. Rica, *Phys. Rev. Lett.* **69**, 1644 (1992).
  - [11] S. Inouye, S. Gupta, T. Rosenband, A. P. Chikkatur, A. Gorlitz, T. L. Gustavson, A. E. Leanhardt, D. E. Pritchard, and W. Ketterle, *Phys. Rev. Lett.* **87**, 080402 (2001).
  - [12] T. W. Neely, E. C. Samson, A. S. Bradley, M. J. Davis, and B. P. Anderson, *Phys. Rev. Lett.* **104**, 160401 (2010).
  - [13] G. Nardin *et al.*, *Nat. Phys.* **7**, 635 (2011).
  - [14] D. Sanvitto *et al.*, *Nat. Phot.* **5**, 610 (2011).
  - [15] G. A. El, A. Gammal, and A. M. Kamchatnov, *Phys. Rev. Lett.* **97**, 180405 (2006).
  - [16] A. M. Kamchatnov and L. P. Pitaevskii, *Phys. Rev. Lett.* **100**, 160402 (2008).
  - [17] A. M. Kamchatnov and S. V. Korneev, *Phys. Lett. A* **375**, 2577 (2011).
  - [18] A. Amo *et al.*, *Science* **332**, 1167 (2011).
  - [19] G. Grosso, G. Nardin, F. Morier-Genoud, Y. Léger, and B. Deveaud-Plédran, *Phys. Rev. Lett.* **107**, 245301 (2011).
  - [20] G. A. El and A. M. Kamchatnov, *Phys. Lett. A* **350**, 192 (2006); **352**, 554(E) (2006).
  - [21] G. A. El, A. M. Kamchatnov, V. V. Khodorovskii, E. S. Annibale, and A. Gammal, *Phys. Rev. E* **80**, 046317 (2009).
  - [22] M. A. Hofer and B. Ilan, *Phys. Rev. A* **80**, 061601(R) (2009).
  - [23] S. Burger, K. Bongs, S. Dettmer, W. Ertmer, K. Sengstock, A. Sanpera, G. V. Shlyapnikov, and M. Lewenstein, *Phys. Rev. Lett.* **83**, 5198 (1999).
  - [24] J. Denschlag *et al.*, *Science* **287**, 97 (2000).
  - [25] R. Onofrio, C. Raman, J. M. Vogels, J. R. Abo-Shaer, A. P. Chikkatur, and W. Ketterle, *Phys. Rev. Lett.* **85**, 2228 (2000).
  - [26] P. Engels and C. Atherton, *Phys. Rev. Lett.* **99**, 160405 (2007).
  - [27] D. Dries, S. E. Pollack, J. M. Hitchcock, and R. G. Hulet, *Phys. Rev. A* **82**, 033603 (2010).
  - [28] L. J. Garay, J. R. Anglin, J. I. Cirac, and P. Zoller, *Phys. Rev. Lett.* **85**, 4643 (2000).
  - [29] S. Giovanazzi, C. Farrell, T. Kiss, and U. Leonhardt, *Phys. Rev. A* **70**, 063602 (2004).
  - [30] C. Barcelo, A. Cano, L. J. Garay, and G. Jannes, *Phys. Rev. D* **74**, 024008 (2006).
  - [31] R. Balbinot, A. Fabbri, S. Fagnocchi, A. Recati, and I. Carusotto, *Phys. Rev. A* **78**, 021603 (2008); I. Carusotto, S. Fagnocchi, A. Recati, R. Balbinot, and A. Fabbri, *New J. Phys.* **10**, 103001 (2008).
  - [32] A. Recati, N. Pavloff, and I. Carusotto, *Phys. Rev. A* **80**, 043603 (2009).
  - [33] J. Macher and R. Parentani, *Phys. Rev. A* **80**, 043601 (2009).
  - [34] P.-É. Larré, A. Recati, I. Carusotto, and N. Pavloff, *Phys. Rev. A* **85**, 013621 (2012).
  - [35] P. Leboeuf and N. Pavloff, *Phys. Rev. A* **64**, 033602 (2001).
  - [36] For a wide barrier the situation is analogous to the flow of a compressible gas through a Laval nozzle.
  - [37] V. Hakim, *Phys. Rev. E* **55**, 2835 (1997).

- [38] N. Pavloff, *Phys. Rev. A* **66**, 013610 (2002).
- [39] A. Radouani, *Phys. Rev. A* **70**, 013602 (2004).
- [40] A. M. Leszczyszyn, G. A. El, Yu. G. Gladush, and A. M. Kamchatnov, *Phys. Rev. A* **79**, 063608 (2009).
- [41] L. D. Landau and E. M. Lifshitz, *Fluid Mechanics* (Pergamon, Oxford, 1987).
- [42] G. Dekel, V. Farberovich, V. Fleurov, and A. Soffer, *Phys. Rev. A* **81**, 063638 (2010).
- [43] C. Menotti and S. Stringari, *Phys. Rev. A* **66**, 043610 (2002).
- [44] M. A. Hoefer, M. J. Ablowitz, I. Coddington, E. A. Cornell, P. Engels, and V. Schweikhard, *Phys. Rev. A* **74**, 023623 (2006).
- [45] R. Meppelink, S. B. Koller, J. M. Vogels, P. vanderStraten, E. D. vanOoijen, N. R. Heckenberg, H. Rubinsztein-Dunlop, S. A. Haine, and M. J. Davis, *Phys. Rev. A* **80**, 043606 (2009).
- [46] A. M. Kamchatnov, *Nonlinear Periodic Waves and Their Modulations—An Introductory Course* (World Scientific, Singapore, 2000).
- [47] G. B. Whitham, *Linear and Nonlinear Waves* (Wiley-Interscience, New York, 1974).
- [48] M. G. Forest and J. E. Lee, Geometry and modulation theory for periodic nonlinear Schrödinger equation, in *Oscillation Theory, Computation, and Methods of Compensated Compactness*, C. Dafermos *et al.*, Eds., IMA Volumes on Mathematics and its Applications 2 (Springer, New York, 1987).
- [49] M. V. Pavlov, *Teor. Mat. Fiz.* **71**, 351 (1987); *Theoret. Math. Phys.* **71**, 584 (1987).
- [50] A. V. Gurevich, A. L. Krylov, and G. A. El, *Sov. Phys. JETP* **74**, 957 (1992).
- [51] A. V. Gurevich and L. P. Pitaevskii, *Sov. Phys. JETP* **38**, 291 (1974).
- [52] R. H. J. Grimshaw and N. Smyth, *J. Fluid Mech.* **169**, 429 (1986).
- [53] N. Smyth, *Proc. R. Soc. London Ser. A* **409**, 79 (1987).
- [54] G. A. El, *Chaos* **15**, 037103 (2005); **16**, 029901 (2006).
- [55] G. A. El kindly informed us that a similar effect has been observed in the numerical study of the evolution of a DSW propagating along a nonuniform background (unpublished).